Bulletin of Geophysics and Oceanography Vol. XX, n. X, pp. xxx-xxx; Xxxxx 20xx
DOI 10.4430/bgo00492

Magnetometry, induced polarisation and direct current resistivity data integration to investigate sulphide mineralisation in the Sar Balla village in Iran

H. Chamani[1], A. Zarean Shirvanehdeh[2], S. Atalou[3] and R. Pourmirzaee[4]

[1] *Department of Civil Engineering, Ahar Branch, Islamic Azad University, Ahar, Iran*
[2] *Department of Civil Engineering, Shabestar Branch, Islamic Azad University, Shabestar, Iran*
[3] *Department of Mining Engineering, Ahar Branch, Islamic Azad University, Ahar, Iran*
[4] *Department of Mining Engineering, Urmia University of Technology, Urmia, Iran*

(Received: 23 November 2024; accepted: 22 May 2025; published online: 15 April 2026)

ABSTRACT Vagueness and non-uniqueness of geophysical data inversion can be reduced through the integration of different geophysical methods. Joint interpretation is one of the most common ways to combine datasets of two or more geophysical methods. In this paper, magnetometry inversion, induced polarisation (IP), and direct current (DC) resistivity data are utilised as a joint interpretation for the investigation of sulphide mineralisation in the Sar Balla village, near Eshghabad city, in Iran. Six profiles with a 100-metre separation are used to collect data. The IP and DC resistivity data are measured using pole-dipole configuration with unit electrode spacings of 20 and 40 m. The damped weighted minimum length solution algorithm is used for inverting both magnetic and DC resistivity data, whereas smoothness constrained inversion is implemented for IP data. Primary investigation using inversion of magnetic data is illustrative of a huge anomaly extending to the north of the profile with a depth range from 100 to 800 m. IP and DC resistivity data enable a more detailed examination of the subsurface down to 300 m, where inverse sections indicate a considerable amount of sulphide mineral deposits with high chargeability and low resistivity. According to these results, 29 regions have high potential for sulphide mineralisation, among which seven anomalies appear to continue to greater depths and can be suggested for deep drilling.

Key words: DC resistivity, induced polarisation, magnetometry, Sar Balla village, sulphide.

1. Introduction

The direct current (DC) resistivity approach is a well-established, cost-effective, and powerful imaging technique to detect subsurface sources. The DC resistivity approach has been extensively implemented for mineral explorations (Shin *et al.*, 2021), hydro-geophysical applications (Ghorbani *et al.*, 2012; Sharafeldin *et al.*, 2019), environmental and engineering purposes (Swileam *et al.*, 2019; Rupesh *et al*., 2024), detecting archaeological targets (Varfinezhad *et al.*, 2020), and volcanology (Fikos *et al.*, 2012). Induced polarisation (IP) can be considered as the most promising geophysical approach for sulphide investigations (Ali *et al.*, 2023), however, it has been used for different practical investigations (Alfouzan *et al*., 2020; Orozco *et al.*, 2022). Magnetometry is a non-destructive and efficient method for the investigation and detection of

anomalies with susceptibility contrasts to their encompassing mediums. This method is one of the most widely used geophysical techniques in mineral explorations (Essa *et al.*, 2022), oil and gas investigations (Al-Farhan *et al.*, 2019), geothermal resources (Zhang *et al.*, 2021), underground water surveys (Al-Gharni *et al.*, 2011), and archaeological studies (Fassbinder, 2023).

Geophysical data can be integrated in three main different ways: 1) joint interpretation (Orlando, 2005; Milano *et al.*, 2021; Ghari *et al.*, 2023), 2) cooperative or sequential inversion (Le *et al.*, 2016; Varfinezhad *et al.*, 2023), in which inversion of one geophysical dataset is manipulated as an initial model for the inversion of another geophysical dataset, and 3) joint inversion which can be categorised into petrophysical-based joint inversion (Ghose and Slob, 2006) and joint inversion based on structural similarities (Gallardo and Meju, 2004; Fregoso and Gallardo, 2009; Gallardo and Meju, 2011; Joulidehsar *et al.*, 2018; Varfinezhad *et al.*, 2020). In joint interpretation, at first the inversions of individual geophysical datasets are obtained, then an interpretation of subsurface targets is made based on the individual inverse models and any other data available, such as geological information, well-logging data, etc. Joint interpretation is a subjective procedure which means two geophysicists may propose two different interpretations. Although this is the main disadvantage of joint interpretation, in most cases this discrepancy is not significant. Therefore, the joint interpretation of geophysical data can be a reliable strategy for the interpretation of subsurface structures (e.g. Orlando, 2005; Al Farajat, 2009; Sultan *et al.*, 2010; Karavul *et al.*, 2010; Gambetta *et al.*, 2011; Orfanos and Apostolopoulos, 2011; Zhang *et al.*, 2018; Ebrahimi *et al.*, 2019; Milano *et al.*, 2021; Parnow *et al.*, 2021; Ghari *et al.*, 2023).

Porphyry deposits are the main origin for copper, molybdenum, and rhenium (Sillitoe, 2010). Since the physical properties of minerals in porphyry deposits appear to be highly variable, different geophysical techniques can be used for their exploration. DC resistivity and IP methods may be used for sulphide minerals, which can be found in a plethora of disparate alteration zones. IP is the most widespread and appropriate geophysical method used to estimate spatial extension of sulphide mineralisation, while DC resistivity is helpful in tracing lithology, alteration, and metallic minerals. The magnetic approach (ground-based and airborne) is another geophysical method which can be helpful in exploring porphyry deposits as, for example, potassic alteration zones are rich of magnetic minerals. However, the same is not true with phyllic alteration zones. Consequently, a magnetic anomaly may be found at a potassic alteration zone which is encompassed by a low magnetic anomaly associated with the phyllic alteration zone (Fatehi and Asadi Haroni, 2019).

In this paper, the joint interpretation of magnetic, IP, and DC resistivity datasets is carried out to investigate the sulphide mineralisation of the Sar Balla village, close to Eshghabad city, in Iran. For this purpose, the damped weighted minimum length solution inversion algorithm is used for magnetic and DC resistivity data, whereas the smoothness constrained inverse technique is applied to IP data. At first, magnetic data are examined and, then, inversion models of IP and DC resistivity data are carried out simultaneously to interpret subsurface anomalies with greater details so as to recognise high-potential anomalies for sulphide mineralisation.

2. Methodology

2.1. Direct current resistivity and induced polarisation data inversions

DC resistivity, like other geophysical methods, can be modelled using finite differences, finite elements, and integral equations. In this paper, the weighted minimum length solution inversion

algorithm presented by Varfinezhad *et al.* (2022) is implemented. They used the integral equation method introduced by Perez-Flores *et al.* (2001) and manipulated the depth weighting function as the model weighting in the inverse procedure.

Perez-Flores *et al.* (2001) presented the following linear integral equation for DC resistivity modelling problems, which relates the logarithm of apparent resistivities (data) to the logarithm of true resistivities (model parameters):

$$\log \rho_a(\boldsymbol{r}_A.\boldsymbol{r}_B.\boldsymbol{r}_M.\boldsymbol{r}_N) = \frac{C}{4\pi^2} \times \int \boldsymbol{M}(\boldsymbol{r}_A.\boldsymbol{r}_B.\boldsymbol{r}_M.\boldsymbol{r}_N.\boldsymbol{r}') \times \log \rho_a(\boldsymbol{r}')\, d^3\, \boldsymbol{r}' \tag{1}$$

where *C* stands for the geometrical factor of the configuration, $\boldsymbol{r_A}$, $\boldsymbol{r_B}$, $\boldsymbol{r_M}$, $\boldsymbol{r_N}$, and $\boldsymbol{r'}$ denote the position vectors of electrodes *A*, *B*, *M*, *N* and anomaly, respectively. $\boldsymbol{M}$ is defined as:

$$\boldsymbol{M}(\boldsymbol{r}_A.\boldsymbol{r}_B.\boldsymbol{r}_M.\boldsymbol{r}_N.\boldsymbol{r}') = \boldsymbol{L}(\boldsymbol{r}_A.\boldsymbol{r}_M.\boldsymbol{r}') - \boldsymbol{L}(\boldsymbol{r}_A.\boldsymbol{r}_N.\boldsymbol{r}') - \boldsymbol{L}(\boldsymbol{r}_B.\boldsymbol{r}_M.\boldsymbol{r}') + \boldsymbol{L}(\boldsymbol{r}_B.\boldsymbol{r}_N.\boldsymbol{r}') \tag{2}$$

where

$$\boldsymbol{L}(\boldsymbol{r}_i.\boldsymbol{r}_j.\boldsymbol{r}') = \frac{(\boldsymbol{r}'-\boldsymbol{r}_i)(\boldsymbol{r}_j-\boldsymbol{r}')}{|\boldsymbol{r}'-\boldsymbol{r}_i|^3|\boldsymbol{r}_j-\boldsymbol{r}'|^3} \quad . \; i = A\,, B \quad and \quad j = M, N. \tag{3}$$

The interested subsurface area is discretised into many prisms with infinite length along the strike direction (Fig. 1) to carry out numerical simulation; therefore, Eq. (1) is reduced to the following matrix equation:

$$\mathbf{d} = \mathbf{A}\mathbf{m} \tag{4}$$

where **d** stands for data vector including observed apparent resistivities, **m** is the model vector, and **A** represents the forward matrix. In order to detect subsurface sources, the damped weighted minimum length solution algorithm is utilised for the inverse process (Varfinezhad *et al.*, 2022):

$$\mathbf{m}_{\boldsymbol{k}} = \mathbf{m}_{k-1} + (\mathbf{W}_m^{-1}\mathbf{A}^{\mathbf{T}})(\mathbf{A}\mathbf{W}_m^{-1}\mathbf{A}^{\mathbf{T}} + \mu \boldsymbol{I})^{-1}(\mathbf{d} - \mathbf{A}\mathbf{m}_{k-1}) \tag{5}$$

where μ is the regularisation parameter, W_m is the depth weighting function, and *I* is the identity matrix.

For IP data inversion, the smoothness constrained algorithm is adopted. In this case, the following objective function is minimised (Loke and Dahlin, 2002):

$$\Psi(\mathbf{m_k}) = \mathbf{g}_{\boldsymbol{k}}^{\boldsymbol{T}}\mathbf{g}_{\boldsymbol{k}} + \mu_k \mathbf{m}_{\boldsymbol{k}}^{\boldsymbol{T}}\mathbf{W_m}\mathbf{m_k} \tag{6}$$

with $\mathbf{W_m} = a_x\mathbf{C_x}^{\mathbf{T}}\mathbf{C_x} + a_z\mathbf{C_z}^{\mathbf{T}}\mathbf{C_z}$ where $\mathbf{C_x}$ and $\mathbf{C_z}$ are smoothness matrices in the *x* and *z* directions, respectively, and α_X, α_Z are the relative weights. $\mathbf{g_k} = \mathbf{d}\text{-}F(\mathbf{m_k})$ is the data misfit vector, and μ_k represents the damping factor. Considering the gradient of the objective function, the smoothness constrained algorithm leads to the following system of equations (Loke and Dahlin, 2002):

$$\left(\mathbf{J}_k^T\mathbf{J}_k + \mu_k\mathbf{W}_\mathbf{m}\right)\Delta\mathbf{m_k} = \mathbf{J}_k^T\mathbf{g}_k - \mu_k\mathbf{W}_\mathbf{m}\mathbf{m_{k-1}} \tag{7}$$

where $\mathbf{J_k}$ is the Jacobian matrix. At first, model variation Δm_k is obtained, then the model is updated as $\mathbf{m}_{k+1} = \mathbf{m}_k + \Delta\mathbf{m}_k$.

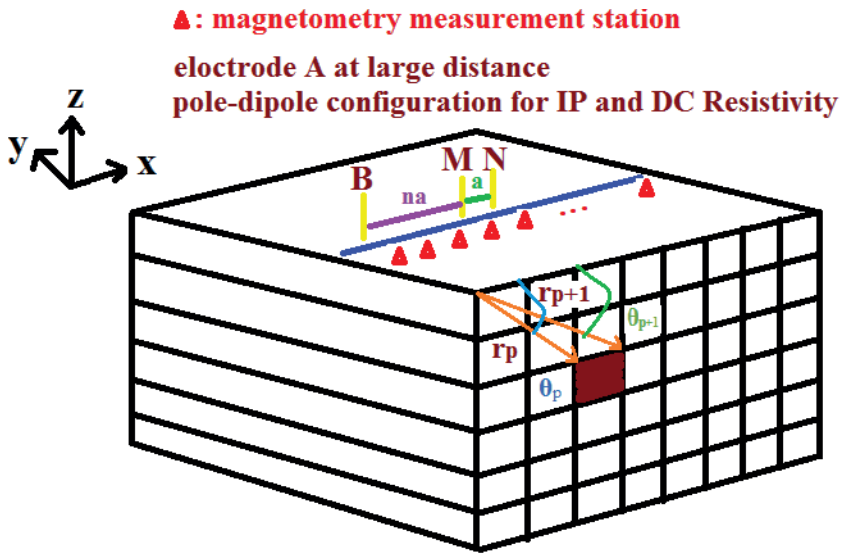

Fig. 1 - The subsurface is divided into many prisms. The pole-dipole array (for DC resistivity and IP measurements) and magnetic measurement stations are displayed.

2.2. Magnetic method

The interested area (Fig. 1) is discretised into *M* prisms with constant susceptibility, which are elongated infinitely along the geological strike (i.e. *y* direction). Two-dimensional magnetometry forward modelling may be expressed utilising the following equations (Blakely, 1996):

$$d_i = \sum_{j=1}^{M}\sum_{l=1}^{4}(\hat{\boldsymbol{f}}_x B_x^l + \hat{\boldsymbol{f}}_z B_z^l)_j\,, \qquad i = 1, 2, \cdots, N \tag{8}$$

where d_i is the total field at the *i*-th observation point, $\hat{\boldsymbol{f}}_x$ and $\hat{\boldsymbol{f}}_z$ stand, respectively, for the unit vectors of the *x* and *z* geomagnetic field components. B_x^l and B_z^l refer to the *x* and *z* elements of the side *l* of *B* which may be derived from the following equation (Blakely, 1996):

$$B_x = -2C_m(\mathbf{M}\cdot\hat{\boldsymbol{n}})\left[\hat{\boldsymbol{s}}_x \log\left(\frac{\boldsymbol{r}_{p+1}}{\boldsymbol{r}_p}\right) - \hat{\boldsymbol{s}}_z(\theta_p - \theta_{p+1})\right]$$

and (9)

$$B_z = -2C_m(\mathbf{M}\cdot\hat{\boldsymbol{n}})\left[\hat{\boldsymbol{s}}_z \log\left(\frac{r_{p+1}}{r_p}\right) + \hat{\boldsymbol{s}}_x(\theta_p - \theta_{p+1})\right].$$

$\boldsymbol{r_p}$, $\boldsymbol{r_{p+1}}$, θ_p, θ_{p+1} are displayed in Fig. 1, **M** and $\hat{n}$ represent the magnetisation vector and the unit

vector perpendicular to each prism, respectively, so that $\hat{s}_x = -\hat{n}_z$, $\hat{s}_z = -\hat{n}_x$ and $C_m = \mu_0/4\pi = 10^{-7}$ in SI system units.

Again, discretisation of the interested area into many horizontal prisms reduces Eq. (8) to the following matrix equation:

$$\mathbf{d} = \mathbf{Am} \tag{10}$$

where **d** describes a column vector of *N* data, the model vector **m** contains *M* unknowns, and **A** is the forward operator.

Many algorithms are available for magnetic data inversion (e.g. Cella and Fedi, 2012; Paoletti *et al.*, 2013; Essa and Elhussein, 2019; Essa *et al.*, 2021), but like the DC resistivity method, the damped weighted minimum length solution method is applied and, for it, the model weighting function () is the depth weighting (Li and Oldenburg, 1996) multiplied by compactness (Last and Kubic, 1983):

$$\mathbf{m} = (\mathbf{W}_m^{-1}\mathbf{A}^{\mathbf{T}})(\mathbf{A}\mathbf{W}_m^{-1}\mathbf{A}^{\mathbf{T}} + \mu\mathbf{I})^{-1}(\mathbf{d}) \tag{11}$$

where μ stands for the regularisation parameter, and **I** is the identity matrix.

The usefulness of this algorithm has been demonstrated for the inversion of potential field data (e.g. Varfinezhad *et al.*, 2020, 2022; Milano *et al.*, 2021; Ghari *et al.*, 2023).

3. Geology of the area

Fig. 2 represents the exploration area (blue rectangle) on a simplified geological map of Iran. The study area is a part of the 1:100,000 scale map of Uzbak-kouh (Fig. 3) which is presented by Anjelini (2007) and Brount *et al.* (2009), based on the modified maps to classify important structural zones of Iran. The interested area is located in Lut Block, which is a part of the central Iranian subcontinent.

In Fig. 3, the location of the study area, represented on the geological map of Uzbak-kouh, mainly corresponds to three units: 1) micaschiste, 2) micaschiste with marble, and 3) conglomerate. It is important to mention that two main faults, visible in a small region, are the main reason of exploration and are indicative of highly effective tectonic events for mineralisation in this area. Blue dashed line trends can indicate potential places for different mineral deposits. In other words, possible mineralisation may be along this direction.

Fig. 4 shows a 1:5,000 scale geological map, whereas 1:2,000 scale geological units display limestone and schist. Penetrated massive bodies of diorite and granodiorite have outcrops in this area. According to this map, iron mineralisation is magnetite with specularite and hematite, which have outcrops in limestone and schist units. In addition to magnetite mineralisation, gold and copper outcrops are present in the area, which can be indicative of massive sulphide in deep parts.

4. Inversion results and interpretation

The Sar Balla village mine is situated NE of Eshghabad city in Khorasan Razavi province. The interested area was first explored using magnetometry survey. Based on geological and

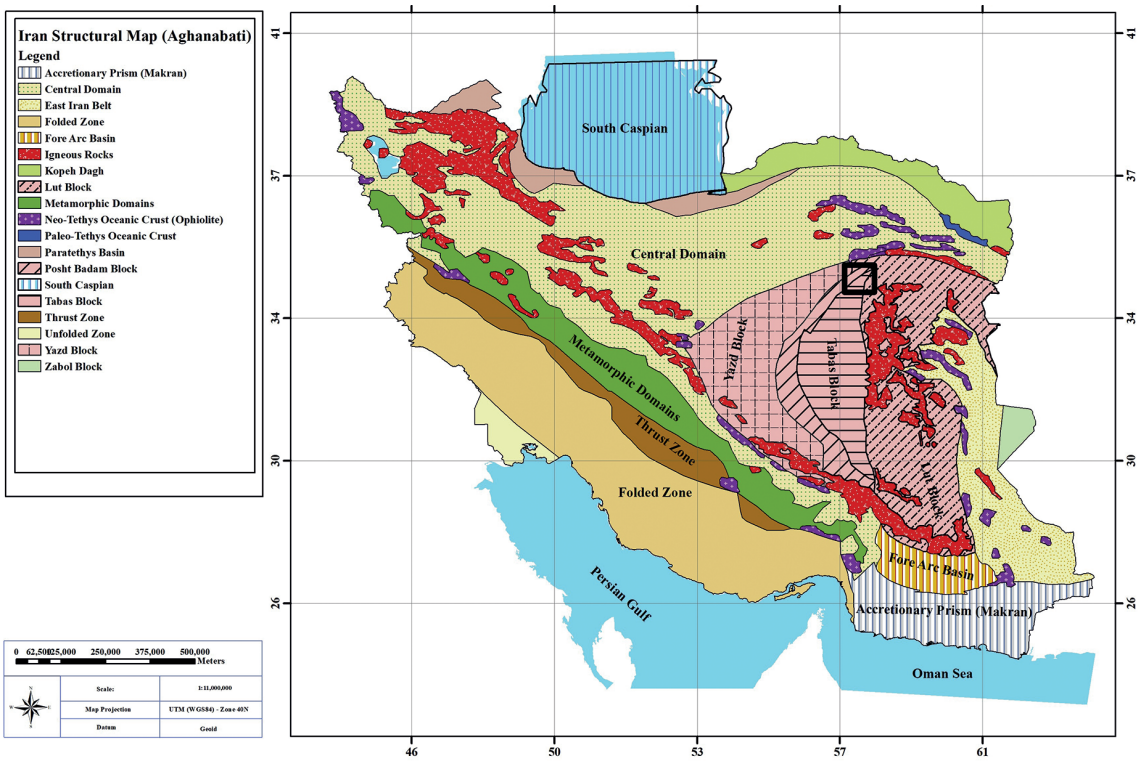

Fig. 2 - Location of the study area (black rectangle) on the geological map of Iran (Aghanabati, 1998).

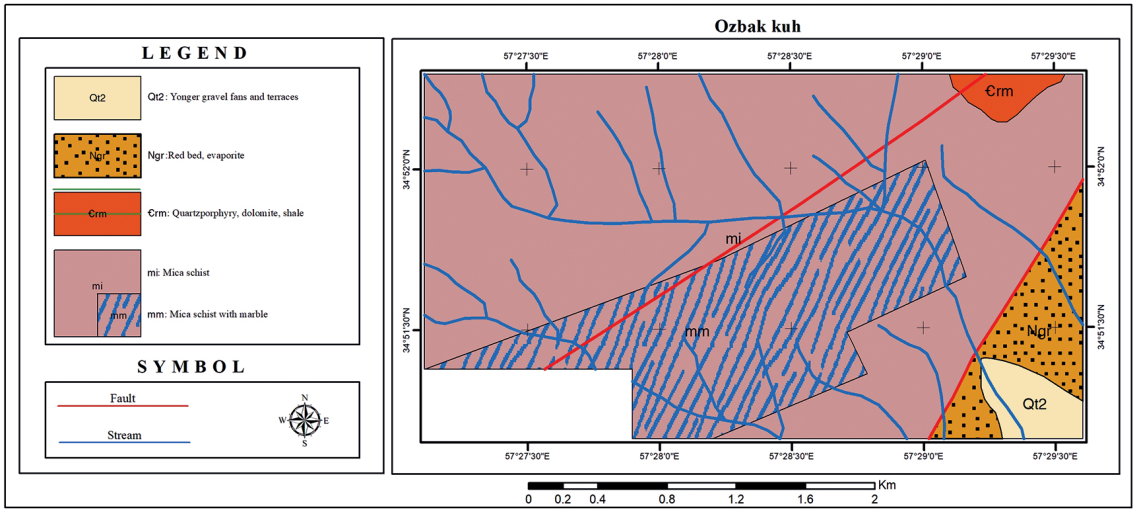

Fig. 3 - Location of the study area on the 1:100,000 scale geological map of Uzbak-kouh (modified from Anjelini, 2007; Brount *et al.*, 2009).

magnetic studies, we decided to investigate the area (within the white box in Fig. 5) in greater detail through DC resistivity and IP methods. This map shows the total magnetic field measured and the profiles (yellow lines). Considering the high potential for sulphide mineralisation of the

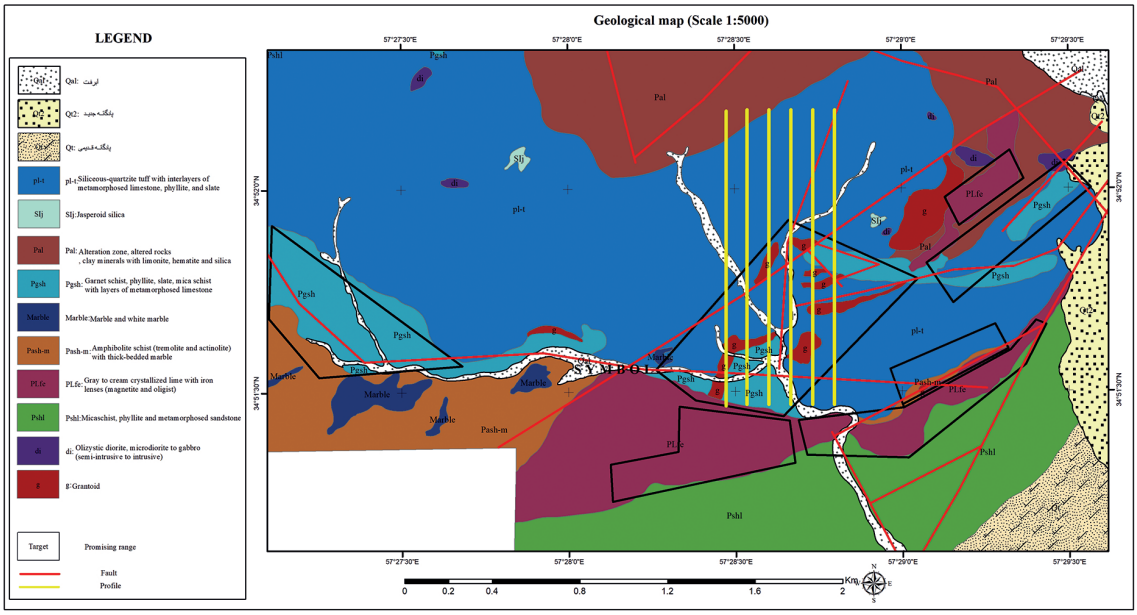

Fig. 4 - 1:5000 scale geological map of the Sar Balla village (Geological Survey of Iran).

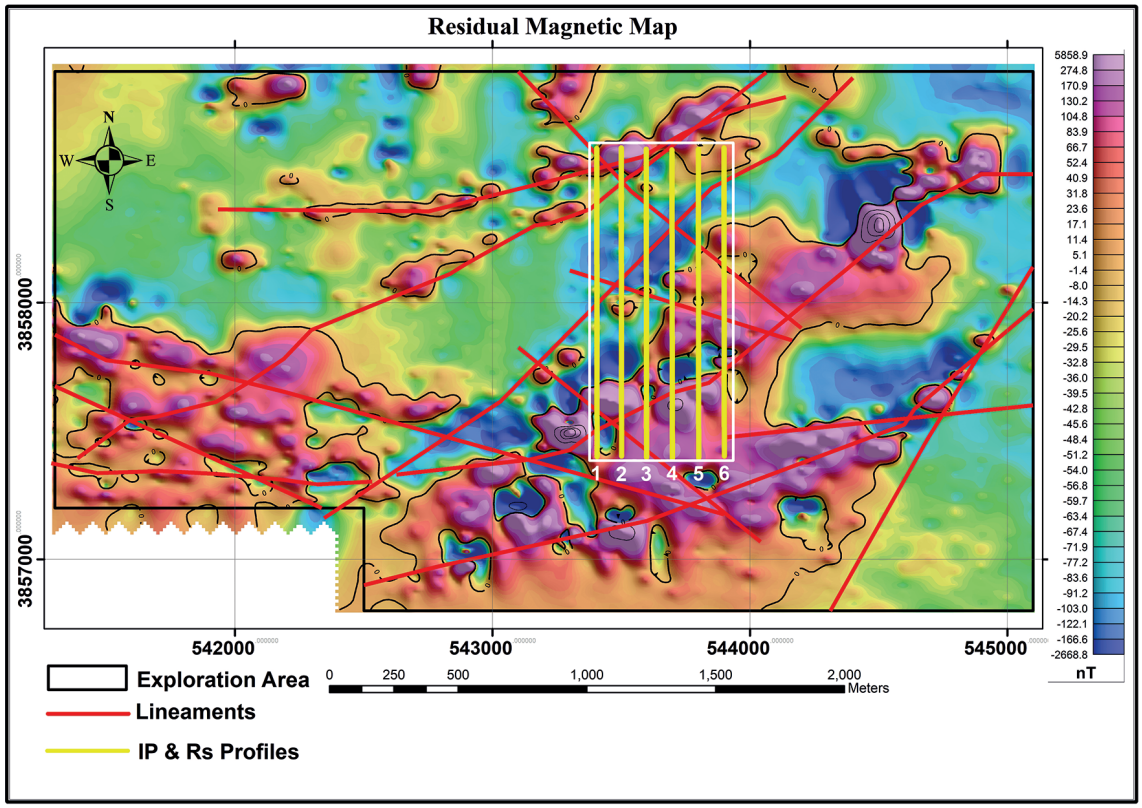

Fig. 5 - The total magnetic field measured in nT. The white rectangle represents the interested block for exploration and the yellow lines show the six profiles.

area, IP and DC resistivity methods were conducted for a more detailed investigation. Based on previous statements, magnetic data inversion is presented first. Data were collected along six profiles with a sample interval of 20 m and a length of 1220 m, while the distance between profiles was 100 m. The subsurface is divided into 61×50 prisms with side lengths of 20 m × 20 m along *x* and *z* directions, respectively. Inversion results of the measured data are displayed in Fig. 6 for these profiles, and measured versus computed data are represented in Fig. 7, expressing a good fit between them. The reconstructed susceptibility model from magnetic data is generally demonstrative of a huge anomaly from depths of 100 to 800 m. One of the most important reasons for investigating this area is the presence of a high susceptibility zone in the low susceptibility zone. The magnetic anomaly, which started from the middle to the end (north) of the profile, is surrounded by the two principal faults of the area. This zone may be suggested as the main anomaly, suitable for deep drilling. From the structural point of view, the magnetic anomaly consists of horsts and grabens, which means mineralisation occurred at considerable depths and is older than the tectonic activities. It should be mentioned that the anomaly in some places is stretched out to near surface and has outcrops.

IP and DC resistivity data are collected using the pole-dipole array with unit electrode spacings of 20 and 40 m along the corresponding magnetic profiles. Distance between profiles and number of data points are 100 m and 8379, respectively.

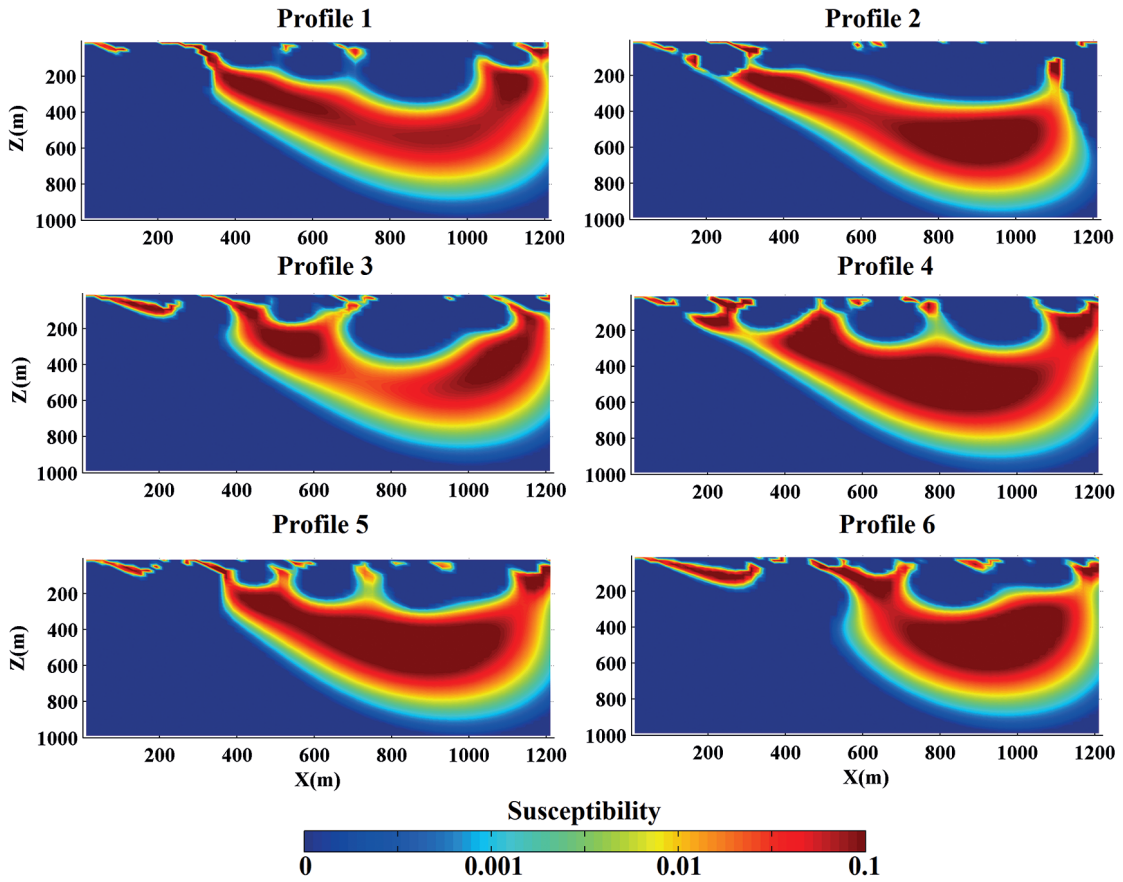

Fig. 6 - Inversion models of the magnetic data along the six profiles.

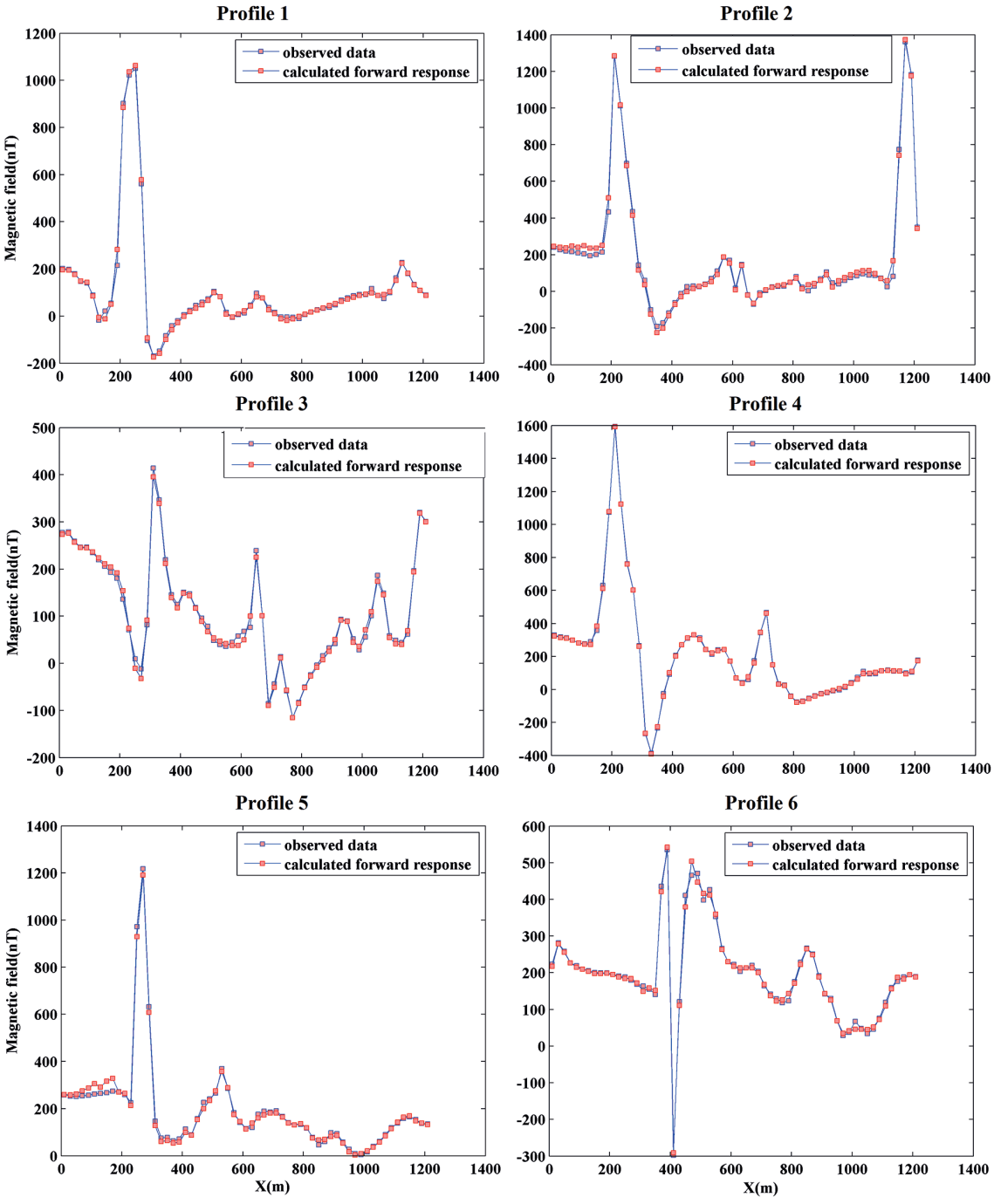

Fig. 7 - Measured and computed data from inversion models represented in Fig. 6.

Before proceeding with the inversion of both IP and DC resistivity data, a static analysis of the measured data is briefly fulfilled. Results of the static analysis are presented in Table 1. For IP data, the minimum and maximum chargeabilities are 2 mV/V and 82.6 mV/V, respectively. After the static analysis, chargeability averages vary from 16 mV/V to 29.4 mV/V and standard deviations cover an interval between 5.6 mV/V and 11.5 mV/V which may be an initial sign and

appropriate criterion for strong sulphide mineralisation. In addition, average and median values of chargeabilities are approximately equal, indicating symmetrical dispersions of the measured data. Apparent resistivities vary from 10 Ω×m to over 1000 Ω×m, but their averages are less than 200 Ω×m. So, we should expect inverse sections with low resistivity backgrounds, which can be another initial signal of sulphide mineralisation, along with high chargeabilities.

Table 1 - Static analysis of measured chargeabilities and apparent resistivities.

Formation number	IP					DC resistivity				
	Min	Max	Average	STD	Median	Min	Max	Average	STD	Median
P1	2.6	36.8	16	5.6	15.6	9	1201	182	105	157
P2	1.3	41.6	16.4	6	15.7	15	1530	197	171	140
P3	1.1	45.4	18	6.2	17.6	6	802	156	101	136
P4	1.5	72.5	20.2	7	20.8	29	1151	163	125	107
P5	1.8	57.5	25.7	9.9	20.6	26	1206	174	151	114
P6	2.0	82.6	29.4	11.5	29.4	14	1575	154	144	103

Inversion models obtained from IP and DC resistivity data are represented in Fig. 8. In general, resistivity sections show very low resistivity values, especially from 400 m to the end of the profiles and usually at large depths, which can be due to shear zones, metallic mineralisation, clayification, and ultimately penetration of brine hydrothermal fluids. Small resistive anomalies are present close to the surface and intermediate depths. Furthermore, a large resistive anomaly is detected at the left sides and large depths of the profiles. Chargeability inverse models show a medium including a few main anomalies, with high chargeability immersed in a low chargeability background. At this point, we investigated all the profiles in more detail, suggesting high potential bodies for sulphide mineralisation.

Desired anomalies representing sulphide are those with high chargeability and low resistivity. Therefore, according to the recovered IP and DC resistivity inverse models, four anomalies (indicated with black ellipses) are highly prone to sulphide mineralisation in profile 1.

Anomaly 3 appears to be appropriate for deep drilling due to its extension to the bottom of the inverse model. The susceptibility model may certify this issue, but borehole dip can be different from -90^0 (e.g. -70^0).

Profile 2 includes six main regions with high potential for sulphide mineralisation. Regions 1, 4, and 6 are composed of one massive body, but regions 2, 3, and 5 are composed of two, three, and four contiguous anomalies, respectively. It can be construed that anomalies 4 and 6 are extended to larger depths, and considering the susceptibility inverse section of profile 2, deep drilling can be a reasonable choice concerning them. Five regions have a high potential for sulphide mineralisation in profile 3, but being anomaly 5 elongated vertically, this potential can be expected to be expanded to much greater depths.

The inverse section of profile 4 is demonstrative of five major anomalies that have a high probability for sulphide mineralisation. Anomaly 3 includes a few relatively small bodies juxtaposed along a depth range that is approximately the same and some with outcrops. Other anomalies have large horizontal and vertical extensions and lie at moderate and deep depths. Anomalies 1, 2, and 5 are stretched to the bottom of the inverse model, but considering the magnetic inversion model associated with this profile as the expression of the continuation of

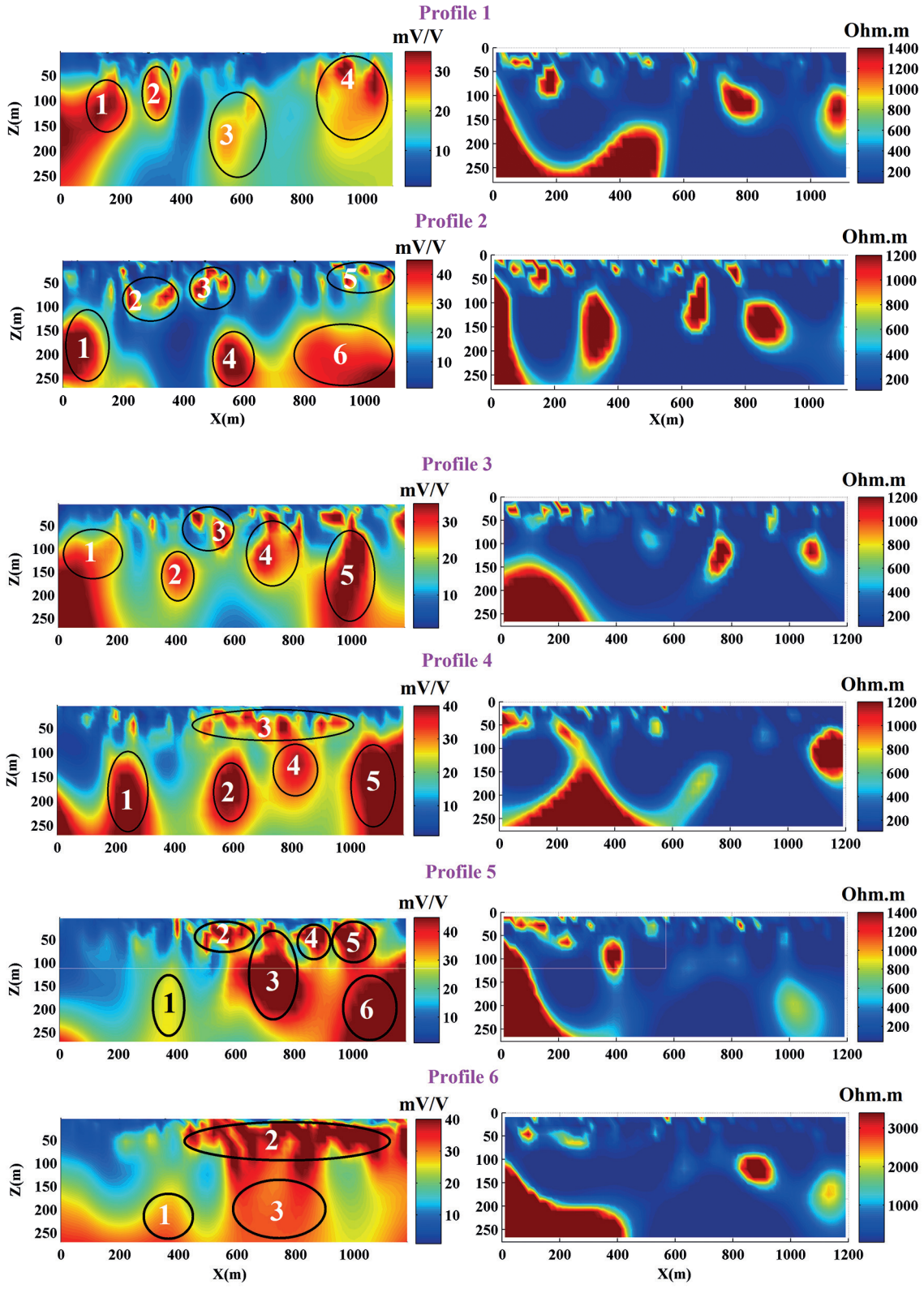

Fig. 8 - Inversion models retrieved from IP (left) and DC resistivity (right) data.

anomaly 2 to very large depths.

Six black ellipses are interpreted as sulphide minerals for profile 5 and three of them have outcrops and are near surface anomalies. Anomaly 3 is situated at a depth range of 100 to 200 m, and the two other anomalies (1 and 6) are extended to the bottom of the inversion model. However, chargeability of anomaly 6 is considerably higher than that of anomaly 1. Compared with the retrieved susceptibility model, the expansion of anomaly 6 to depths larger than 300 m is far more logical.

The chargeability and resistivity sections of profile 6 may suggest three regions for sulphide mineralisation. Anomalies 1 and 3 are in the deepest part of the area, with a relatively lower chargeability than anomaly 2. Anomaly 2 has outcrops and starts horizontally from 400 to 1100 m and enlarges to depths of 70 m and, in some parts, even more than 100 m. The susceptibility model provides strong evidence that anomaly 3 continues to considerable depth.

Figs. 9 and 10 respectively display measured and computed data from inverse models for both DC resistivity and IP methods. It can be concluded that the misfits of computed data in both cases and for all profiles are satisfactory, expressing the good performance of the manipulated inversion codes. However, low root mean squared errors of computed data from inverse models are not necessarily indicative of obtaining the best possible models from measured data, but they can be a criterion to show that reliable inverse models are obtained. This issue is far more persuasive with regards to DC resistivity and IP methods than magnetic approaches, as the non-uniqueness degrees of such methods are far lower than that of magnetic methods (Varfinezhad *et al.*, 2020).

Table 2 - The main drawbacks of the research and their solutions.

Drawbacks	Solutions
Finding an appropriate location for a detailed investigation	Considering geology and implementation of magnetometry
Considering the anomalies that can be considered as sulphide mineralisation	High chargeabilities (IP) and low resistivities (DC resistivity)
Depth of investigation (IP and DC resistivity enabled to examine depths up to about 250 m)	Magnetometry enabled to investigate a depth about 1000 m

5. Conclusions

In this paper, the joint interpretation of magnetometry, IP, and DC resistivity data were used to investigate sulphide mineralisation in the Sar Balla village, situated near Eshghabad city, in Iran. Data for all these methods were collected along six profiles with a 100-metre profile interval. The damped weighted minimum length solution algorithm is applied to DC resistivity and magnetic data but smoothness constrained inversion is implemented for IP data. At first, magnetometry data were inverted, detecting a very large anomaly with a depth range from 100 to 800 m in the northern half of the inverse sections for all the profiles. Subsequently, inverse models of IP and DC resistivity data were scrutinised for more details, resulting in the following findings (Table 2): 1) resistivity models have a low resistivity background including some resistive bodies from near surface to moderate depths and a large resistive anomaly on the left side of the resistivity sections, 2) IP inverse sections have a few small and relatively large bodies with

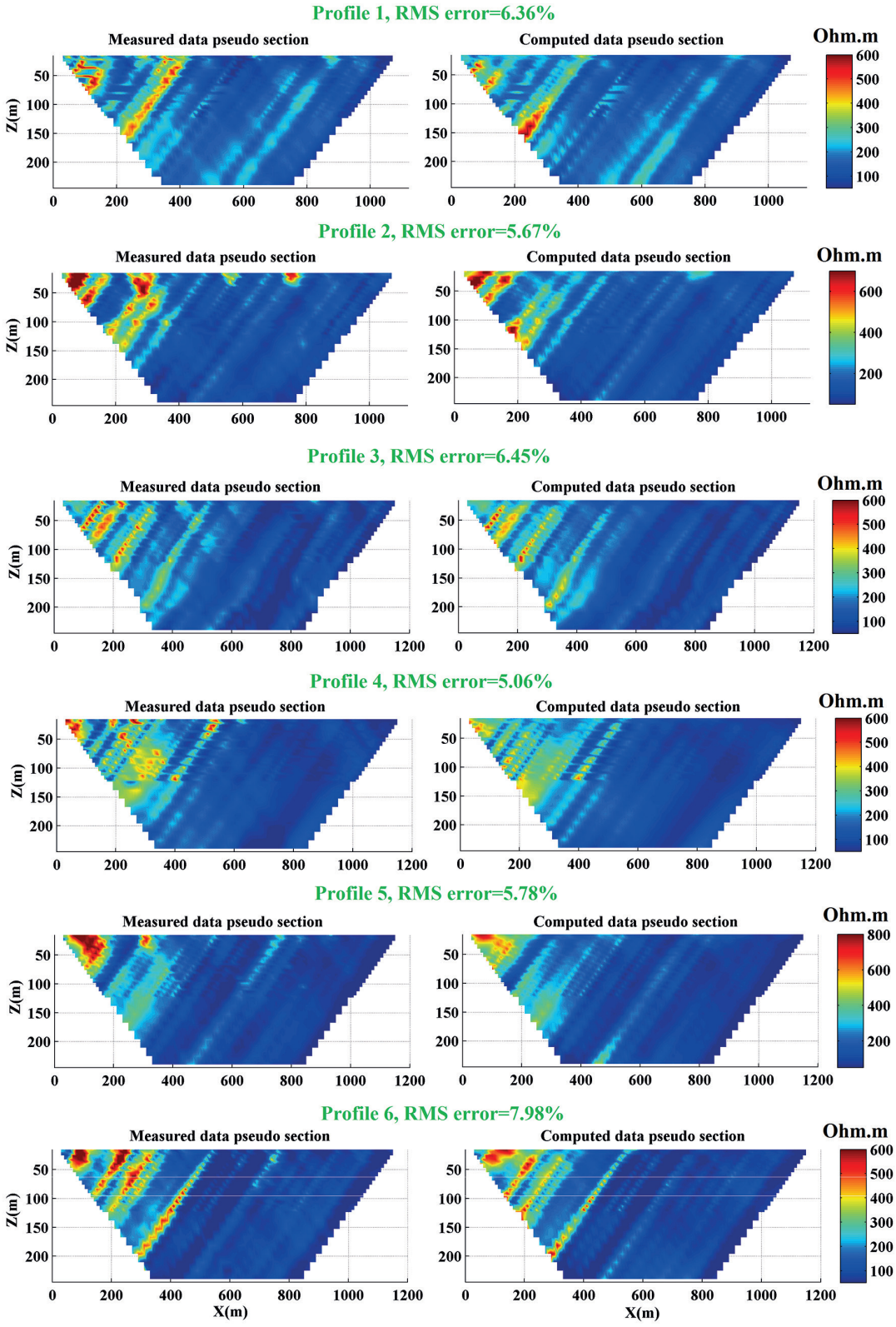

Fig. 9 - Measured apparent resistivities (left) and computed apparent resistivities (right) for all six profiles.

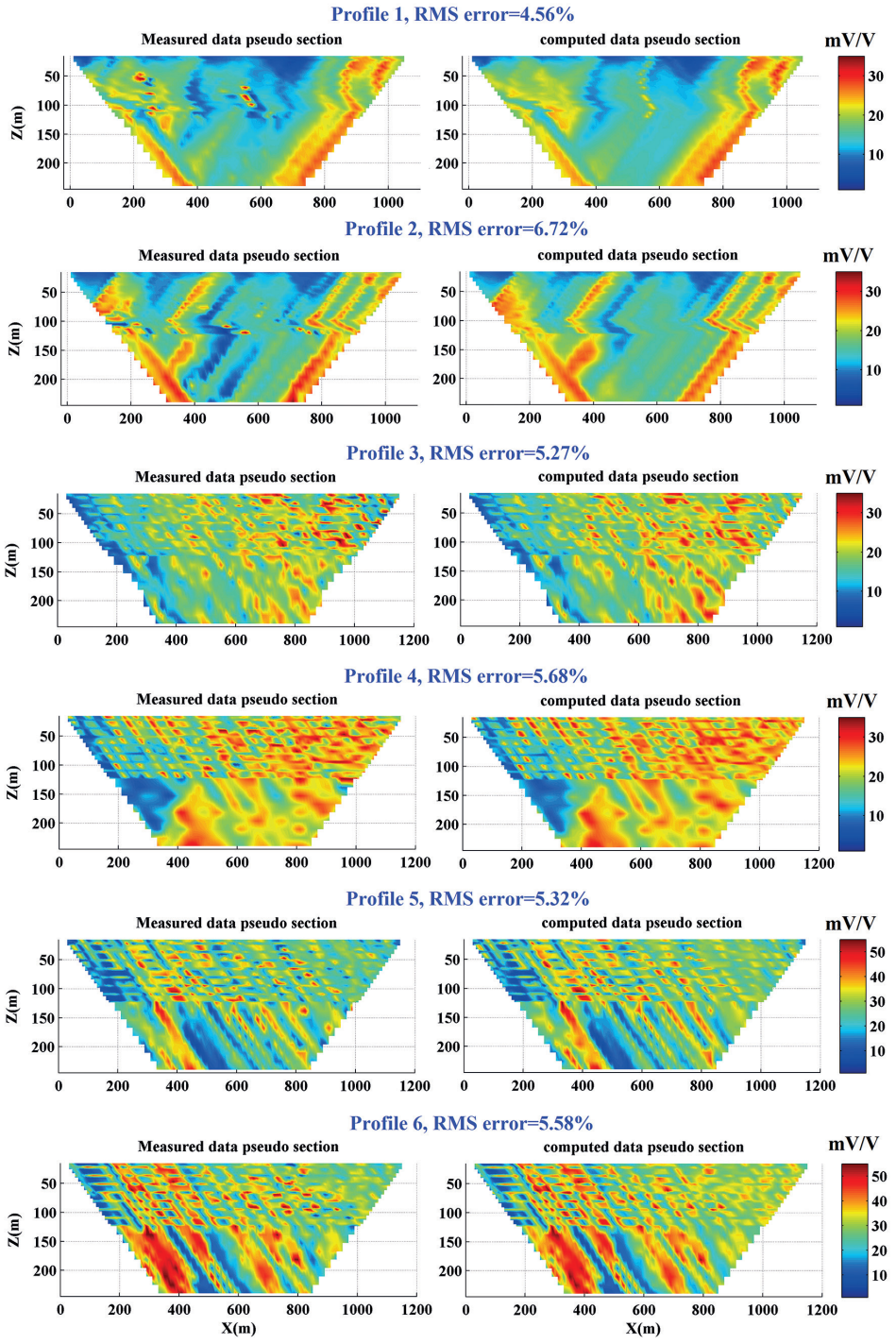

Fig. 10 - Measured apparent chargeabilities and computed apparent chargeabilities for all the profiles.

high chargeabilities which correspond to low resistivity regions which are indicative of sulphide mineralisation, and 3) 29 anomalies were suggested to be sulphide mineralisation for which seven of them, located in the northern half of the profiles, appear to be expanded to very large

depths, consistently with magnetic data inversion which enables to recover subsurface up to considerably greater depths compared to both IP and DC resistivity.

REFERENCES

Aghanabati A.; 1998: *Major sedimentary and structural units of Iran (map).* Geosciences, 7, 29-30.

Al Farajat M.; 2009: *Characterization of a coastal aquifer basin using gravity and resistivity methods: a case study from Aqaba in Jordan.* Acta Geophys., 57, 454-475.

Al-Farhan M., Oskooi B., Ardestani V.E., Abedi M. and Al-Khalidy A.; 2019: *Magnetic and gravity signatures of the Kifl oil field in Iraq.* J. Pet. Sci. Eng., 183, 106397.

Al-Garni M.A. and El-Kaliouby H.M.; 2011: *Delineation of saline groundwater and sea water intrusion zones using transient electromagnetic (TEM) method, Wadi Thuwal area, Saudi Arabia.* Arabian Journal of Geosciences, 4, 655-668, doi: 10.1007/s12517-009-0094-5.

Alfouzan F.A., Alotaibi A.M., Cox L.H. and Zhdanov M.S.; 2020: *Spectral induced polarization survey with distributed array system for mineral exploration: case study in Saudi Arabia.* Miner., 10, 769.

Ali M.A.H., Mewafy F.M., Qian W., Alshehri F., Ahmed M.S. and Saleem H.A.; 2023: *Integration of electrical resistivity tomography and induced polarization for characterization and mapping of (Pb-Zn-Ag) sulfide deposits*. Miner., 13, 986.

Anjelini A.; 2007: *Geological map of Uzbak-kouh, scale 1:100,000.* Geological Survey of Iran, Tehran.

Blakely R.J.; 1996: *Potential theory in gravity and magnetic applications.* Cambridge University Press, Cambridge, UK, 441 pp., doi: 10.1017/CBO9780511549816.

Brunet M.-F., Wilmsen M. and Granath J.W. (eds); 2009): *South Caspian to central Iran basins.* Geological Society Special Publication No. 312, Geological Society, London, UK.

Cella F. and Fedi M.; 2012: *Inversion of potential field data using the structural index as weighting function rate decay*. Geophys. Prospect., 60, 313-336.

Ebrahimi A., Dehghan M.J. and Ashtari A.; 2019: *Contribution of gravity and Bristow methods for Karez (aqueduct) detection*. J. Appl. Geophys., 161, 37-44.

Essa K.S. and Elhussein M.; 2019: *Magnetic interpretation utilizing a new inverse algorithm for assessing the parameters of buried inclined dike-like geological structure*. Acta Geophys., 67, 533-544.

Essa K.S., Mehanee S. and Elhussein M.; 2021: *Magnetic data profiles interpretation for mineralized buried structures identification applying the variance analysis method*. Pure Appl. Geophys., 178, 973-993.

Essa K.S., Munschy M., Youssef M.A.S. and Khalaf E.; 2022: *Aeromagnetic and radiometric data interpretation to delineate the structural elements and probable precambrian mineralization zones: a case study. Egypt.* Min., Metall. Explor., 39, 2461-2475, doi: 10.1007/s42461-022-00675-0.

Fassbinder J.W.E.; 2023: *Magnetometry for archaeology.* In: Gilbert A.S., Goldberg P., Mandel R.D. and Aldeias V. (eds), Encyclopedia of Geoarchaeology, Encyclopedia of Earth Sciences Series, Springer, Cham, Switzerland, doi: 10.1007/978-3-030-44600-0_169-1.

Fatehi M. and Asadi Haroni H.; 2019: *Geophysical signatures of the gold rich porphyry copper deposits: a case study at the Dalli Cu-Au porphyry deposit.* J. Econ. Geol., 10, 639-675.

Fikos I., Vargemezis G., Zlotnicki J., Puertollano J.R., Alanis P.B., Pigtain R.C. and Sasai Y.; 2012: *Electrical resistivity tomography study of Taal volcano hydrothermal system, Philippines.* Bull. Volcanol., 74, 1821-1831, doi: 10.1007/s00445-012-0638-5.

Fregoso E. and Gallardo L.A.; 2009: *Cross gradients joint 3D inversion with applications to gravity and magnetic data*. Geophys., 74, 31-42.

Gallardo L.A. and Meju M.A.; 2004: *Joint two-dimensional DC resistivity and seismic travel time inversion with cross gradients constraints*. J. Geophys. Res.: Solid Earth, 109, B03311.

Gallardo L.A. and Meju M.A.; 2011: *Structure coupled multiphysics imaging in geophysical sciences*. Rev. Geophys., 49, RG1003, doi:10.1029/2010RG000330.

Gambetta M., Armadillo E., Carmisciano C., Stefanelli P., Cocchi L. and Tontini F.C.; 2011: *Determining geophysical properties of a near-surface cave through integrated microgravity vertical gradient and electrical resistivity tomography measurements*. J. Cave and Karst Studies, 73, 11-15.

Ghari H., Varfinezhad R. and Parnow S.; 2023: *3D joint interpretation of potential field, geology, and well data to evaluate a salt dome in the Qarah-Aghaje area, Zanjan, NW Iran.* Near Surf. Geophys., 21, 233-246.

Ghorbani A., Ali Ghari H. and Namiranian A.; 2012: *Electrical resistivity monitoring of rock samples during uniaxial compression test*. Iran. J. Geophys., 6, 34-41.

Ghose R. and Slob E.C.; 2006: *Quantitative integration of seismic and GPR reflections to derive unique estimates for water saturation and porosity in subsoil.* Geophys. Res. Lett., 33, doi: 10.1029/2005GL025376.

Joulidehsar F., Moradzadeh A. and Doulati Ardejani F.; 2018: *An improved 3D joint inversion method of potential field data using cross-gradient constraint and LSQR method*. Pure Appl. Geophys., 175, 4389-4409.

Karavul C., Dedebali Z., Keskinsezer A. and Demirkol A.; 2010: *Magnetic and electrical resistivity image survey in a buried Adramytteion ancient city in western Anatolia, Turkey.* Int. J. Phys. Sci., 5, 876-883.

Last B.J. and Kubik K.; 1983: *Compact gravity inversion.* Geophys., 48, 713-721.

Le C.V.A., Harris B., Pethick A.M., Takougang E.M.T. and Howe B.; 2016: *Semiautomatic and automatic cooperative inversion of seismic and magnetotellurics data*. Surv. Geophys, 37, 845-896.

Li Y. and Oldenburg D.W.; 1996: *3-D inversion of magnetic data.* Geophys., 61, 394-408.

Loke M.H. and Dahlin T.; 2002: *A comparison of the Gauss–Newton and quasi-Newton methods in resistivity imaging inversion.* J. Appl. Geophys., 49, 149-162, doi: 10.1016/S0926-9851(01)00106-9.

Milano M., Varfinezhad R., Bizhani H., Moghadasi M., Kalateh A.N. and Baghzendani H.; 2021: *Joint interpretation of magnetic and gravity data at the Golgohar mine in Iran.* J. Appl. Geophys., 195, 104476.

Orlando L.; 2005: *Joint interpretation of geophysical data for archaeology. A case study.* Subsurf. Sens. Tech. Appl., 6, 235-250.

Orfanos C. and Apostolopoulos G.; 2011: *2D-3D resistivity and microgravity measurements for the detection of an ancient tunnel in the Lavrion area, Greece*. Near Surf. Geophys., 9, 449-457.

Orozco A.F., Steiner M., Katona T., Roser N., Moser C., Stumvoll M.J. and Glade T.; 2022: *Application of induced polarization imaging across different scales to understand surface and groundwater flow at the Hofermuehle landslide.* Catena, 219, 106612.

Paoletti V., Ialongo S., Florio G., Fedi M. and Cella F.; 2013: *Self-constrained inversion of potential fields.* Geophys. J. Int., 195, 854-869.

Parnow S., Oskooi B. and Florio G.; 2021: *Improved linear inversion of low induction number electromagnetic data.* Geophys. J. Int., 224, 1505-1522.

Perez-Flores M.A., Méndez-Delgado S. and Gomez-Treviño E.; 2001: *Imaging low frequency and DC electromagnetic fields using a simple linear approximation.* Geophys., 66, 1067-1081.

Rupesh R., Tiwari P. and Sharma S.P.; 2024: *Estimation of geotechnical parameters for coal exploration from quasi-3D electrical resistivity measurements.* Miner., 14, 102, doi: 10.3390/min14010102.

Sharafeldin S.M., Essa K.S., Youssef M.A., Karsli H., Diab Z.E. and Sayil N.; 2019: *Shallow geophysical techniques to investigate the groundwater table at the great pyramids of Giza, Egypt.* Geosci. Instrum., Methods and Data Systems, 8, 29-43.

Shin Y., Shin S., Cho S.J. and Son J.S.; 2021: *Application of 3D electrical resistivity tomography in the Yeoncheon titanomagnetite deposit, south Korea.* Miner., 11, 563, doi: 10.3390/min11060563.

Sillitoe R.H.; 2010: *Porphyry copper systems.* Econ. Geol., 105, 3-41.

Sultan S.A., Santos F.A.M. and Abbas A.M.; 2010: *Joint inversion interpretation for gravity and resistivity data: a case study at New Heliopolis city, Cairo, Egypt.* Near Surf. Geophys., 8, 43-53.

Swileam G.S., Shahin R.R., Nasr H.M. and Essa K.S.; 2019: *Spatial variability assessment of Nile alluvial soils using electrical resistivity technique.* Eurasian J. Soil Sci., 8, 110-117.

Varfinezhad R., Oskooi B. and Fedi M.; 2020: *Joint inversion of DC resistivity and magnetic data, constrained by cross gradients, compactness and depth weighting.* Pure Appl. Geophys., 177, 4325-4343.

Varfinezhad R., Fedi M. and Milano M.; 2022: *The role of model weighting functions in the gravity and DC resistivity inversion.* IEEE Trans. Geosci. Remote Sens., 60, 1-15.

Varfinezhad R., Parnow S., Florio G., Fedi M. and Mohammadi Vizheh M.; 2023: *DC resistivity inversion constrained by magnetic method through sequential inversion.* Acta Geophys., 71, 247-260.

Zhang G., Lu Q.T. and Zhang G.B.; 2018. *Joint interpretation of geological, magnetic, AMT, and ERT data for mineral exploration in the northeast of inner Mongolia, China.* Pure Appl. Geophys., 175, 989-1002.

Zhang J., Hao T., Dong M., Xu Y., Wang B., Ai Y. and Fang G.; 2021: *Investigation of geothermal structure of the Sulawesi, using gravity and magnetic method.* Sci. China Earth Sci., 64, 278-293.

Corresponding author: Ahmad Zarean Shirvanehdeh
Department of Civil Engineering, Shabestar Branch, Islamic Azad University
Shahrdari Boulevard, Shabestar, Iran
Phone: +98 4142425311; e-mail: Ah.zarean@iau.ac.ir